

EPSC2018

OPS6/TP17/EX08 abstracts

Impact of Crustal Magnetic Fields on the Thermal Structure of the Martian Upper Atmosphere

Jun Cui (1,2,3), Roger Yelle (4), Shane Stone (4), Tommi Koskinen (4), Xiaoshu Wu (2) and Lingling Zhao (5)

- (1) School of Atmospheric Sciences, Sun Yat-sen University, Zhuhai, Guangdong, China
- (2) National Astronomical Observatories, Chinese Academy of Sciences, Beijing, China
- (3) Lunar and Planetary Science Laboratory, Macau University of Science and Technology, Macau, China
- (4) Lunar and Planetary Laboratory, University of Arizona, Tucson, AZ, USA
- (5) Center for Space Plasma and Aeronomic Research, University of Alabama in Huntsville, Huntsville, AL, USA

Abstract

Using the MAVEN Neutral Gas and Ion Mass Spectrometer (NGIMS) data, we investigate the possible impact of crustal magnetic fields on the thermal structure of the Martian upper atmosphere. Our analysis reveals a clear enhancement in temperature over regions with strong crustal magnetic fields during two Deep Dip (DD) campaigns covering the periods of 17-22 Apr and 2-8 Sep, both in 2015. Several controlling factors, such as solar EUV irradiance, relative atomic O abundance, and non-migrating tides, do not help to explain the observed temperature enhancement, and a magnetically driven scenario is favored. We evaluate the roles of several heating mechanisms that are likely modulated by the presence of crustal magnetic fields, including Joule heating, ion chemical heating, as well as electron impact heating via either precipitating Solar Wind electrons or locally produced photoelectrons. The respective heating rates of these mechanisms are substantially lower than the solar EUV heating rate, implying that none of them is able to interpret the observations.

1. Introduction

The thermal structure of the dayside Martian upper atmosphere is controlled by solar EUV heating, radiative cooling via CO₂ emission at 15 μ m, and thermal conduction (Bougher & Roble 1991). The role of solar forcing has been confirmed by a number of authors using the data from the drag experiments made onboard Mars Global Surveyor (MGS) (Forbes et al. 2008, Krasnopolsky 2010), and the data acquired by the Neutral Gas and Ion Mass Spectrometer (NGIMS), the Accelerometer (ACC), as well as the Imaging Ultraviolet Spectrograph (IUVS) onboard the Mars Atmosphere and Volatile Evolution (MAVEN)

spacecraft (Mahaffy et al. 2015, Jain et al. 2015, Zurek et al. 2017, Bougher et al. 2017).

In addition to solar EUV radiation, solar wind (SW) electron precipitation likely provides an additional heat source for regions with open magnetic field lines. This implies that the temperature in the Martian upper atmosphere is potentially modulated by the strong crustal magnetic fields over the southern hemisphere of the planet (Acuna et al. 1999). Crustal magnetic fields may also affect the local thermal balance either via Joule heating (Vasyliunas & Song 2005) or via trapping of photoelectrons (Harada et al. 2016). In addition, crustal magnetic fields likely affect local plasma distribution (Andrews et al. 2014) and accordingly local heating via exothermic ion chemistry (Fox 1988). Search for the impact of crustal magnetic fields on the thermal structure of the dayside Martian upper atmosphere was attempted based on the dayglow emission data acquired by the Mars Express (MEX) Spectroscopy for the Investigation of the Characteristics of the Atmosphere of Mars (SPICAM), but no firm conclusion was reached (Leblanc et al. 2006, Stiepen et al. 2015).

At the nightside, the thermal structure of the Martian upper atmosphere is less constrained by observations (Schofield et al. 1997). Analysis of the Mars Pathfinder (MPF) Atmospheric Structure Investigation (ASI) accelerometer data yielded a peak nightside temperature of 153 K at 134 km (Magalhaes et al. 1999). SW electron precipitation likely plays an essential role as the dominant heating mechanism, replacing solar EUV heating at the dayside, as motivated by numerous studies of the nightside ionosphere of Mars, both observationally (Withers et al. 2012) and theoretically (Lillis et al. 2009). Energy deposition by precipitating electrons may also be accomplished via the transport of dayside photoelectrons to the nightside under favorable magnetic field configurations (Xu et al. 2016). In both

cases, an impact of crustal magnetic fields on nightside temperature is expected.

2. Summary and Conclusions

With the aid of the extensive measurements made by the MAVEN NGIMS instrument, we examine in this study whether the observed temperature variability in the Martian upper atmosphere could be magnetically driven. Specifically, by analyzing the MAVEN NGIMS measurements of CO₂ during several DD campaigns that sample the southern hemisphere of Mars, we are able to compare the mean temperature profiles obtained over regions with strong crustal magnetic fields and those obtained over regions without. We observe clear temperature enhancement over crustal magnetic fields for one subsolar campaign (DD2) and another near-terminator campaign (DD4). The temperature enhancement is manifest over a limited altitude range, centered around 155 km for DD2 and 170 km for DD4. Several controlling factors, such as solar EUV irradiance, relative atomic O abundance, and non-migrating tides, do not help to explain the observed temperature enhancement, and a magnetically driven scenario is favored.

We evaluate the roles of several heating mechanisms that are likely modulated by the presence of crustal magnetic fields by calculating the respective heating rates and comparing them to the solar EUV heating rates. These mechanisms include Joule heating, ion chemical heating, as well as electron impact heating via either precipitating SW electrons or locally produced photoelectrons. None of these mechanisms is able to interpret the NGIMS observations.

Despite this, we caution that the influence of near-terminator Joule heating could be large if the horizontal plasma flow velocity reaches $> 1 \text{ km s}^{-1}$ as implied by some previous studies of day-to-night transport in the Martian ionosphere (Cui et al. 2015).

Conclusions made in the present study rely exclusively on the NGIMS measurements made during two DD campaigns. Further support is clearly required to confirm the impact of crustal magnetic fields on neutral temperature, as well as to identify the responsible mechanism when more data become available. For this purpose, the data from the MAVEN nominal science orbits may not be very useful since the impact of magnetic field is likely manifest at altitudes below their periapses. This is in contrast to the recent finding that a similar impact on electron

temperature is manifest above 200 km (Flynn et al. 2017).

Acknowledgements

JC acknowledges supports from the National Science Foundation of China (NSFC) through grants 41525015, 41774186, and 41504133. This work is also supported by the Science and Technology Development Fund of Macau SAR (FDCT) through grants 039/2013/A2 and 082/2015/A3.

References

- [1] Acuna, M.H., et al., 1999, *Science*, 284, 790
- [2] Andrews, D.J., et al., 2014, *JGR*, 119, 3944
- [3] Bougher, S.W. & Roble, R.G., 1991, *JGR*, 96, 11
- [4] Bougher, S.W., et al., 2017, *JGR*, 122, 1296
- [5] Cui, J., et al., 2015, *JGR*, 120, 2333
- [6] Flynn, C.L., et al., 2017, *GRL*, 44, 10812
- [7] Forbes, J.M., et al., 2008, *GRL*, 35, L01201
- [8] Fox, J.L., 1988, *P&SS*, 36, 37
- [9] Harada, Y., et al., 2016, *GRL*, 43, 939
- [10] Jain, S.K., et al., 2015, *GRL*, 42, 9023
- [11] Krasnopolsky, V.A., 2010, *Icarus*, 207, 638
- [12] Leblanc, F., et al., 2006, *JGR*, 111, E09S11
- [13] Lillis, R.J., et al., 2009, *JGR*, 114, E11009
- [14] Magalhaes, J.A., et al., 1999, *JGR*, 104, 8943
- [15] Mahaffy, P.R., et al., 2015, *GRL*, 42, 8951
- [16] Schofield, J.T., et al., 1997, *Science*, 278, 1752
- [17] Stiepen, A., et al., 2015, *Icarus*, 245, 295
- [18] Vasyliunas, V.M., & Song, P., 2005, *JGR*, 110, A02301
- [19] Withers, P., et al., 2012, *JGR*, 117, A12307
- [20] Xu, S., et al., 2016, *GRL*, 43, 8876
- [21] Zurek, R.W., et al., 2017, *JGR*, 122, 3798

A large grid of super-Earth upper atmosphere models and its application to planetary evolution

Daria Kubyshkina (1), Luca Fossati (1), Nicolay Erkaev (2,3), Colin Johnstone (4), Patricio Cubillos (1), Kristina Kislyakova (4,1), Helmut Lammer (1), Monika Lendl (1,5) and Petra Odert (1)

(1) Space Research Institute, Austrian Academy of Sciences, Schmiedlstrasse 6, A-8042 Graz, Austria, (2) Institute of Computational Modelling, FRC “Krasnoyarsk Science Center SB RAS”, 660036, Krasnoyarsk, Russian Federation, (3) Siberian Federal University, 660041, Krasnoyarsk, Russian Federation, (4) Institute for Astronomy, University of Vienna, Türkenschanzstrasse 17, A-1180 Vienna, Austria, (5) Max Planck Institute for Astronomy, Königstuhl 17, 69117 Heidelberg, Germany (daria.kubyskhina@oeaw.ac.at)

Abstract

The NASA Kepler mission revealed the existence of a large variety of planets very different from what we know from the Solar System. Among them a large number of planets was found in the range between Earth and Neptune (e.g. [1]), with a large spread in average densities (e.g. [2-4]). These planets are easier to detect and characterize in comparison to Earth-like planets, making them primary targets for a number of upcoming missions such as CHEOPS [5], TESS [6], JWST [7], PLATO [8], and ARIEL [9].

As part of the work carried out in support to the scientific preparations for the CHEOPS mission, we have assembled a large grid of upper planetary atmosphere models covering super-Earths hosting hydrogen-dominated atmospheres and orbiting early M- to late F-type main-sequence stars. The planetary mass ranges between 1 and 39 Earth masses (up to twice Neptune mass), while the radii cover the 1 to 10 Earth radii (up to 2.5 Neptune radius) range. The equilibrium temperature of the planets spans from 300 to 2000 K. For each stellar mass, we considered three distinct values of the high-energy (XUV) stellar fluxes, which cover roughly the interval from a chromospherically active to a quiet star.

The base physical model is an upgraded version of the model from [10], that is a 1D hydrodynamic model of an XUV-heated atmosphere accounting for hydrogen dissociation, recombination and ionization, $\text{Ly}\alpha$ - and H_3^+ -cooling, and X-ray heating. The boundaries are the planet photosphere and Roche lobe. To allow the computation of a large grid, the XUV stellar spectrum is simplified to two wavelength points: 60 nm and 5 nm for the emission in the extreme ultraviolet (EUV) and X-ray spectral ranges, respectively.

The grid of models consists of about 7000 points and provides the height profiles of the main atmospheric parameters, namely temperature, velocity, bulk density and hydrogen species fractions, from which we compute the atmospheric escape rates and other relevant quantities. We further developed an interpolation routine allowing one to obtain the output of the model grid for any planet lying inside the grid boundaries.

We coupled the interpolation routine with a planetary structure code providing the atmospheric mass fractions for any given planet on the basis of the system parameters and basic assumptions [13]. By employing the two codes, we compute planetary atmosphere evolution tracks for a number of known planets. We further employ the MESA Isochrones and Stellar Tracks (MIST; [11]) to account for changes of stellar temperature, radius (controlling the planetary equilibrium temperature), and bolometric luminosity (involved in the computation of the stellar XUV flux [12]).

We present the modelling scheme, the code upgrades, the model grid, and the interpolation routine. We further show how the current lack of a hydrogen-dominated atmosphere for close-in, high-density super-Earths can be the result of atmospheric escape. We finally apply our simple atmospheric evolution scheme to planets hosting a hydrogen-dominated atmosphere showing how it can lead to further constraining important planetary and stellar properties.

Acknowledgements

We acknowledge the Austrian Forschungsförderungsgesellschaft FFG project “TAPAS4CHEOPS” P853993, the Austrian Science

Fund (FWF) NFN project S11607-N16, and the FWF project P27256-N27. NVE acknowledges support by the RFBR grant No. 15-05-00879-a and 16-52-14006ANF_a.

References

- [1] Mullally, F., Coughlin, J. L., Thompson, S. E., et al. 2015, *ApJS*, 217, 31
- [2] Lopez, E. D., & Fortney, J. J. 2014, *ApJ*, 792, 1
- [3] Wolfgang, A., Rogers, L. A., & Ford, E. B. 2016, *ApJ*, 825, 19
- [4] Cubillos, P., Erkaev, N. V., Juvan, I., et al. 2017a, *MNRAS*, 466, 1868
- [5] Broeg, C., Fortier, A., Ehrenreich, D., et al. 2013, *European Physical Journal Web of Conferences*, 47, 03005
- [6] Ricker, G. R., Winn, J. N., Vanderspek, R., et al. 2015, *Journal of Astronomical Telescopes, Instruments, and Systems*, 1, 014003
- [7] Deming, D., Seager, S., Winn, J., et al. 2009, *PASP*, 121, 952
- [8] Rauer, H., Catala, C., Aerts, C., et al. 2014, *Experimental Astronomy*, 38, 249
- [9] Tinetti, G., Drossart, P., Eccleston, P., et al. 2017, *European Planetary Science Congress*, 11, EPSC2017-713
- [10] Erkaev, N. V., Lammer, H., Odert, P., et al. 2016, *MNRAS*, 460, 1300
- [11] Paxton, B., Schwab, J., Bauer, E. B., et al. 2018, *ApJS*, 234, 34
- [12] Mamajek, E. E., & Hillenbrand, L. A. 2008, *ApJ*, 687, 1264-1293
- [13] Johnstone et al. (2015).

Ionization Efficiency in the Dayside Martian Upper Atmosphere

Xiaoshu Wu (1), Jun Cui (1,2,3) and Shaosui Xu (4)

(1) National Astronomical Observatories, Chinese Academy of Sciences, Beijing, China

(2) School of Atmospheric Sciences, Sun Yat-sen University, Zhuhai, Guangdong, China

(3) Lunar and Planetary Science Laboratory, Macau University of Science and Technology, Macau, China

(4) Space Science Laboratory, University of California at Berkeley, Berkeley, CA, USA

Abstract

Combining the Mars Atmosphere and Volatile Evolution (MAVEN) measurements of neutral atmospheric density, solar EUV/X-ray flux, and differential photoelectron intensity made during 240 nominal orbits, we calculate the ionization efficiency, defined as the ratio of the secondary (photoelectron impact) ionization rate to the primary (photon impact) ionization rate, in the dayside Martian upper atmosphere under a range of solar illumination conditions. Both the CO₂ and O ionization efficiencies tend to be constant from 160 km up to 250 km, with respective median values of 0.19 ± 0.03 and 0.27 ± 0.04 . These values are useful for fast calculation of the ionization rate in the dayside Martian upper atmosphere, without the need to construct photoelectron transport models. No substantial diurnal and solar cycle variations can be identified, except for a marginal trend of reduced ionization efficiency as approaching the terminator. Our analysis further reveals a connection between regions with strong crustal magnetic fields and regions with high ionization efficiencies, likely indicative of more efficient vertical transport of photoelectrons near magnetic anomalies.

1. Introduction

The Martian ionosphere contains at the dayside a well-defined primary layer and a low altitude secondary layer which are produced by solar EUV/X-ray ionization along with impact ionization by photoelectrons (Withers 2009 and references therein). These processes are parameterized by the primary and secondary ionization rates, respectively, with the ratio of the latter to the former being frequently termed as ionization efficiency (Richards & Torr 1988). The calculation of the primary ionization rate is straightforward with the aid of the classical Beer-

Lambert law, whereas the calculation of the secondary ionization rate, which requires either the implementation of the Monte Carlo algorithm (Bhardwaj & Jain 2009) or the multi-stream solution to the Boltzmann equation (Wedlund et al. 2011), is far more involved.

The ionization efficiency in the dayside upper atmosphere was calculated for the Earth (Lilensten et al. 1989), Titan (Lilensten et al. 2005), Mars (Nicholson et al. 2009), Saturn (Galand et al. 2009), as well as giant exoplanets such as HD 209458b (Ionov et al. 2014). In each of the aforementioned works, a photoelectron transport model was coupled with a neutral background atmosphere model to compare the primary and secondary ionization rates under a range of solar illumination conditions. Empirical formulae for these model-based ionization efficiencies were provided in some of the existing works, allowing fast calculation of the total ionization rates in the dayside ionospheres of selected planetary bodies.

Since information on ionization efficiency is crucial for aeronomical studies, it is instructive to validate the model results of this key parameter with real data. This was not feasible for Mars until the arrival of the Mars Atmosphere and Volatile Evolution (MAVEN) mission (Jakosky et al. 2015), which provides a unique opportunity to explore a wide parameter space of controlling factors required for calculating both primary and secondary ionization rates in the dayside Martian upper atmosphere. These controlling factors include solar EUV/X-ray flux, measured by the Extreme Ultraviolet Monitor (EUVM) (Eparvier et al. 2015), the neutral atmospheric density, measured by the Neutral Gas and Ion Mass Spectrometer (NGIMS) (Mahaffy et al. 2015), as well as the differential electron intensity, measured by the Solar Wind Electron Analyzer (SWEA) (Mitchell et al. 2016). The above sources of data are utilized in this study to

determine the ionization efficiency, which is then compared with existing model results (Fox & Yeager 2006, Haider et al. 2006, Nicholson et al. 2009).

2. Summary and Conclusions

Combining the NGIMS, EUVM, and SWEA measurements of neutral atmospheric density, solar EUV/X-ray flux, and differential photoelectron intensity made during 240 nominal MAVEN orbits, we calculate the ionization efficiency, defined as the ratio of the secondary ionization rate to the primary ionization rate, in the dayside Martian upper atmosphere under a range of solar illumination conditions. The photoelectron energy spectra are corrected for spacecraft charging using the MAVEN Langmuir Probe and Waves (LPW) potentials (Andersson et al. 2015), and a portion of the spectra showing strong fluctuations at the top of the atmosphere, likely indicative of significant energy input via Solar Wind (SW) electron precipitation, are excluded. This ensures a clean selection of orbits where secondary ionization is predominantly caused by photoelectrons. The data from the dayside DD campaign on 17-22 Apr 2015, as well as the outbound data from all nominal orbits, are excluded to reduce the effect of NGIMS wall chemistry.

Our analysis reveals that both the CO₂ and O ionization efficiencies remain constant over the altitude range of 160 km to 250 km. No substantial diurnal and solar cycle variations are suggested by the data, except for an insignificant trend of reduced ionization efficiency as approaching the terminator. At the top of the atmosphere, the median ionization efficiencies are 0.19 ± 0.03 for CO₂ and 0.27 ± 0.04 for O, respectively, in fair agreement with various model results covering a range of solar irradiance levels from low to high solar activities and a range of solar illumination angles from subsolar to near-terminator (e.g., Fox & Yeager 2006, Haider et al. 2006, Nicholson et al. 2009). These values are useful for fast calculations of the total ionization rate in the dayside Martian upper atmosphere, without the need to construct photoelectron transport models. A tentative trend of enhanced ionization efficiency is observed near the periapsis of nominal MAVEN orbits. The inclusion of extra data gathered during dayside DD campaigns, along with a rigorous treatment of NGIMS wall chemistry, is required to pin down the vertical trend at low altitudes unambiguously.

Our analysis also reveals a connection between regions with strong crustal magnetic fields and regions with relatively high ionization efficiencies. One possible interpretation is the trapping of in-situ produced photoelectrons by closed magnetic field lines typically found over strong crustal magnetic anomalies (Brain et al. 2007). Since photoelectrons also play a crucial role in the local energy balance of both neutrals and thermal electrons, we expect enhanced neutral and electron temperatures encountered near magnetic anomalies as well. The observation of enhanced neutral temperature was reported by Cui et al. (2018) with the aid of the NGIMS data acquired during several DD campaigns, but these authors argued that photoelectron trapping was unlikely to be a viable mechanism since the difference in photoelectron impact heating between regions with and without strong crustal magnetic fields was far insufficient to account for the difference in neutral temperature. Meanwhile, Flynn et al. (2017) showed that regions over magnetic anomalies featured low electron temperatures, in contrast to our ideal expectation. According to Xu et al. (2017), the magnetic field configuration throughout the entire atmospheric regions of interest here is dominated by closed field lines, indicating that photoelectrons are always trapped at these altitudes irrespective of the magnetic field strength. However, the same authors concluded that the field lines in regions with strong magnetic fields were more vertical as compared to regions with weak fields. Therefore, it is more likely a higher tendency for vertical photoelectron transport that is responsible for the observed enhancement in ionization efficiency near strong crustal anomalies. For comparison, a higher tendency for vertical diffusion is thought to contribute to the enhanced thermal electron content in the Martian upper atmosphere also observed near crustal anomalies (Ness et al. 2000, Nielsen et al. 2007, Safaeinili et al. 2007), as supported by the model calculations of Matta et al. (2015). Clearly, the construction of realistic photoelectron transport models with properly imposed ambient magnetic field topology is required to interpret unambiguously the observed impact of crustal fields on ionization efficiency.

Acknowledgements

JC acknowledges supports from the National Science Foundation of China (NSFC) through grants 41525015, 41774186, and 41504133. This work is also supported by the Science and Technology Development Fund of Macau SAR (FDCT) through grants 039/2013/A2 and 082/2015/A3.

References

- [1] Andersson, L., et al., 2015, SSR, 195, 173
- [2] Bhardwaj, A., & Jain, S.K., 2009, JGR, 114, A11309
- [3] Brain D.A., et al., 2007, JGR, 112, A09201
- [4] Cui et al., et al., 2018, ApJL, 853, L33
- [5] Eparvier, F.G., et al., 2015, SSR, 195, 293
- [6] Flynn, C.L., et al., 2017, GRL, 44, 10
- [7] Fox, J.L., & Yeager, K.E., 2006, JGR, 111, A10309
- [8] Galand, M., et al., 2009, JGR, 114, A06313
- [9] Haider, S.A., et al., 2006, Icarus, 185, 102
- [10] Ionov, D.E., et al., 2014, SSR, 48, 105
- [11] Jakosky, B.M., et al., 2015, GRL, 42, 8791
- [12] Lilensten, J., et al., 1989, AG, 7, 83
- [13] Lilensten, J., et al., 2005, Icarus, 174, 285
- [14] Mahaffy, P.R., et al., SSR, 195, 49
- [15] Matta, M., et al., 2015, JGR, 120, 766
- [16] Mitchell, D.L., et al., 2016, SSR, 200, 495
- [17] Ness, N.F., et al., 2000, JGR, 105, 15991
- [18] Nicholson, W.P., et al., 2009, MNRAS, 400, 369
- [19] Nielsen, E., et al., 2007, P&SS, 55, 2164
- [20] Richards, P.G., & Torr, D.G., 1988, JGR, 93, 4060
- [21] Safaeinili, A., et al., 2007, GRL, 34, L23204
- [22] Wedlund, C.S., et al., 2011, AG, 29, 187
- [23] Withers, P., 2009, ASR, 44, 277
- [24] Xu, S., et al., 2017, JGR, 122, 1831

CUTE: A Small NUV Satellite Mission to Study Exoplanet Atmospheres

Luca Fossati (1), Kevin France (2), Brian Fleming (2), Sreejith Aickara Gopinathan (1), Arika Egan (2), Jean-Michel Desert (3), Tommi Koskinen (4), Pascal Petit (5) and Aline Vidotto (6)

(1) Austrian Academy of Sciences, Space Research Institute, Graz, Austria (luca.fossati@oeaw.ac.at), (2) University of Colorado, Laboratory for Atmospheric and Space Physics, Boulder, Colorado, United States (3) Anton Pannekoek Institute for Astronomy, University of Amsterdam, Netherlands (4) University of Arizona, Lunar and Planetary Laboratory, Tucson, Arizona, United States (5) Université de Toulouse, IRAP, CNRS, CNES, UPS, Toulouse, France (6) University of Dublin, Trinity College Dublin, School of Physics, Dublin, Ireland

Abstract

Exoplanets in short-period orbits provide a unique opportunity to observe phenomena critical to the development and evolution of our own solar system, including atmospheric escape, interaction with the host star, and the potential to study exoplanetary magnetism. At present, the theories explaining atmospheric mass-loss exceed the number of relevant transit observations because these processes cannot be observed in broad-band visible/NIR light curves. Owing to their large sizes and short-periods, the physics of atmospheric mass-loss can be studied with a dedicated small instrument operating in the near-ultraviolet. We present the Colorado Ultraviolet Transit Experiment (CUTE), a 6U CubeSat mission that will spectrally isolate diagnostic atomic and molecular transitions arising within the upper planetary atmospheres to study the physics of atmospheric escape and possibly detect the presence of magnetic fields on exoplanets. CUTE is planned for launch in mid-2020, with a baseline survey program designed to observe about 10 transits of approximately 12 bright exoplanetary systems. We further present the CUTE data simulator, which is a versatile tool easily adaptable to any other mission performing single slit spectroscopy and carrying on-board a CCD detector. CUTE's flexible observing plan also allows for coordinated UV-optical-infrared observations of particularly interesting bright targets with a number of current and future facilities. Detailed information about CUTE can be found in Fleming et al. (2018; [1]).

project ACUTEDIRNDL P859718. CUTE is supported by NASA grant NNX17AI84G (PI - K. France) to the University of Colorado Boulder.

References

- [1] Fleming, B. T., France, K., Nell, N., et al. 2018, *Journal of Astronomical Telescopes, Instruments, and Systems*, 4, 014004

Acknowledgements

L.F. and S.A.G. acknowledge financial support from the Austrian Forschungsförderungsgesellschaft FFG

The near-UV transmission spectrum of the prototypical hot Jupiter HD 209458 b

Luca Fossati (1), Patricio Cubillos (1), Tommi Koskinen (2), Kevin France (3), Monika Lendl (1) and Sreejith Aickara Gopinathan (1)

(1) Austrian Academy of Sciences, Space Research Institute, Graz, Austria (luca.fossati@oeaw.ac.at), (2) University of Arizona, Lunar and Planetary Laboratory, Tuscon, Arizona, United States (3) University of Colorado, Laboratory for Atmospheric and Space Physics, Boulder, Colorado, United States

Abstract

There is growing observational and theoretical evidence suggesting that atmospheric escape is a key driver of planetary evolution, thus shaping the observed exoplanet demographics. We present how the near-ultraviolet (NUV) spectral range offers ample possibilities to directly observe and constrain the properties of exoplanet upper atmospheres. To date, WASP-12 and HD 209458 are the only systems with observed and published spectrally resolved NUV transit observations collected with HST [2, 3, 4]. The first analysis of the prototypical hot Jupiter HD 209458 NUV observations, concentrated exclusively on the analysis of two Mg features, led to an unexpected result with respect to the Mg ionisation balance in the planetary upper atmosphere. However, past experience with far-UV transit observations has shown that analyses of the same data-sets carried out in different ways may lead to significantly different results. Therefore, we carried out an independent re-analysis of the HST NUV transit observations of HD 209458 b and present here its results. We partially confirm the previous result and show how our re-analysis may lead to resolving the tension between observations and modelling with respect to the Mg ionisation balance. We further show that the transmission spectrum displays a number of previously undetected planetary absorption features that help constrain the physical conditions of the planetary upper atmosphere. We finally show how in the near future the CUTE Small Satellite mission [1], focused on the collection of NUV transmission spectra, will significantly improve our general knowledge of atmospheric escape and of circumplanetary environments.

Acknowledgements

L.F. and S.A.G. acknowledge financial support from the Austrian Forschungsförderungsgesellschaft FFG project ACUTEDIRNDL P859718. CUTE is supported by NASA grant NNX17AI84G (PI - K. France) to the University of Colorado Boulder.

References

- [1] Fleming, B. T., France, K., Nell, N., et al. 2018, *Journal of Astronomical Telescopes, Instruments, and Systems*, 4, 014004
- [2] Fossati, L., Haswell, C. A., Froning, C. S., et al. 2010, *ApJL*, 714, L222
- [3] Haswell, C. A., Fossati, L., Ayres, T., et al. 2012, *ApJ*, 760, 79
- [4] Vidal-Madjar, A., Huitson, C. M., Bourrier, V., et al. 2013, *A&A*, 560, A54

An empirical model of Saturn's thermosphere based on Cassini/UVIS occultations

Tommi T. Koskinen (1), Darrell F. Strobel (2), Zarah L. Brown (1)

(1) Lunar and Planetary Laboratory, University of Arizona, Arizona, USA, (2) Morton K. Blaustein Department of Earth and Planetary Sciences, Johns Hopkins University, Maryland, USA (tommi@lpl.arizona.edu)

Abstract

Stellar and solar occultations obtained by the Cassini/UVIS instrument constitute the most extensive dataset on a giant planet upper atmosphere to date. These observations cover different latitudes and times during the 13-year duration of the Cassini mission, ranging from 2005 until the end of mission in 2017. They allow for the retrieval of the H₂ density and temperature structure of the thermosphere and constrain temporal variability. We present an empirical model designed to match these data that will be made available to the community in order to enable access to the retrieved temperatures and densities. The result is a useful constraint on models of Saturn's upper atmosphere and a necessary input for models of the ionosphere and, for example, dayglow and auroral emissions. It will also be a useful tool in planning of future missions to study Saturn's atmosphere.

1. Introduction

The Cassini/UVIS instrument observed more than 70 stellar occultations and more than 20 solar occultations between 2005 and the end of the Cassini mission in 2017. Stellar occultations are observed simultaneously in the EUV and FUV channels [1] and used to retrieve temperature and densities for H₂, CH₄ and some minor hydrocarbons in the mesosphere and thermosphere [2, 3]. Solar occultations are observed in the EUV channel and used to retrieve temperature and densities of H₂ and CH₄ in the thermosphere [4]. They also provide an upper limit on H densities near the exobase. The observations cover different times and latitudes from the equator to the poles. In particular, more than 30 stellar occultations were obtained in 2016 and 2017 that provide a snapshot of meridional trends in the upper atmosphere. We present an empirical model that matches the H₂ density and temperature in the thermosphere. The uncertainties in this model represent the variability of the atmosphere over time.

2. Methods

Saturn is the most oblate of the giant planets in the solar system and therefore, our model is given in oblate spheroidal coordinates [5]. This approach allows us to identify density and temperature trends without interference from the general shape of the pressure density levels. Occultations in the EUV channel yield H₂ density and temperature as a function of planetocentric latitude and radial distance from Saturn's center. The latitude probed does not change significantly during occultations and the profiles are vertical for practical purposes. The oblate spheroidal 'altitude' coordinate ξ is defined so that the family of curves for which $\xi = \text{constant}$ forms a system of confocal ellipses. The oblate spheroidal latitude Φ is different from planetocentric latitude. The transformation from a system of radial distances r and planetocentric latitudes ϕ_{pc} to the oblate spheroidal coordinates is:

$$\cosh \xi = \frac{d_1 + d_2}{2f} \quad (1)$$

$$\cos \Phi = \frac{d_1 - d_2}{2f} \quad (2)$$

$$d_1 = \sqrt{r^2 + 2rf \cos(\phi_{pc}) + f^2} \quad (3)$$

$$d_2 = \sqrt{r^2 - 2rf \cos(\phi_{pc}) + f^2} \quad (4)$$

$$f = \epsilon R_S \quad (5)$$

where f is the focal distance, ϵ is the eccentricity of the Saturn ellipsoid and R_S is the equatorial radius. Note that our fits to the data in these coordinates assume zonal symmetry, justified by Saturn's relatively fast rotation.

3. Summary and conclusions

Our results constrain the shape of the density levels in the thermosphere and temperature as a function of latitude and height. For example, Figure 1 shows density as a function of spheroidal latitude for

$\cosh \xi = 2.3675396$ based on occultations from 2005-2015. This density level corresponds to an equatorial radius and altitude of 61592 km and 1324 km, respectively. The dashed line is a preliminary model fit to the data. We note that oblate spheroidal coordinates set up a system of second order confocal ellipsoids of revolution or Clairaut spheroids (i.e., the gravitational potential is defined by zonal harmonic J_2). If the density levels conformed with this shape, we would expect the density to be constant along surfaces of constant ξ . The deviations in Figure 1 represent the combination of higher order terms (J_4 , J_6 , ...) in gravitational potential and meridional trends in the thermosphere. We will provide a similar fit to the data at all altitudes that will incorporate all of the available occultations.

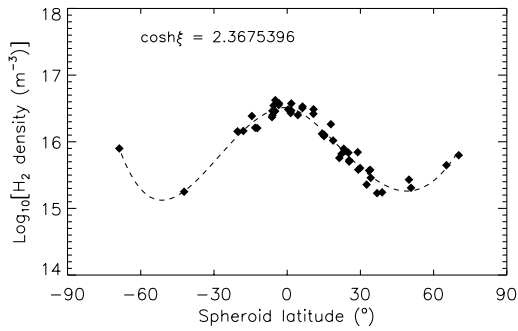


Figure 1: Retrieved occultation densities (diamonds) from 2005-2015 corresponding to an equatorial altitude of 1324 km as a function of spheroidal latitude Φ . The dashed line is a fourth order polynomial fit.

References

- [1] Esposito, L. W., et al.: The Cassini Ultraviolet Imaging Spectrograph investigation, *Space Sci. Rev.*, Vol. 115, pp. 299-361, 2004.
- [2] Koskinen, T. T., Sandel, B. R., Yelle, R. V., Strobel, D. F., Müller-Wodarg, I. C. F., Erwin, J. T.: Saturn's variable thermosphere from Cassini/UVIS occultations, *Icarus*, Vol. 260, pp. 174-189, 2015.
- [3] Koskinen, T. T., Moses, J. I., West, R. A., Guerlet, S., Jouchoux, A.: The detection of benzene in Saturn's upper atmosphere. *GRL*, Vol. 43, pp. 7895-7901, 2016.
- [4] Koskinen, T. T., Sandel, B. R., Yelle, R. V., Capalbo, F. J., Holsclaw, G. M., McClintock, W. E., Edgington, S.: The density and temperature structure near the exobase

of Saturn from Cassini/UVIS solar occultations, *Icarus*, Vol. 226, pp. 1318-1330, 2013.

- [5] Gates, W. L.: Derivation of the equations of atmospheric motion in oblate spheroidal coordinates, *J. Atmos. Sci.*, Vol. 61, pp. 2478-2487, 2004.

Modeling the Upper Atmospheres of Exoplanets: Energy Deposition and Escape

Alex Gloer (1,2), Ofer Cohen (3), Vladimir Airapetian (1,2), Katherine Garcia-Sage (1,2), Guillaume Gronoff (4), Suk-Bin Kang (1,2), and William Danchi (1,2)

(1) Heliophysics Science Division, NASA GSFC, Greenbelt, MD 20771 (2) GSFC Sellers Exoplanet Environments Collaboration, NASA GSFC, Greenbelt, MD 20771 (3) Lowell Center for Space Science and Technology, U. of Massachusetts Lowell, 600 Suffolk Street, Lowell, MA 01854 (4) Science Systems and Application, Inc. & NASA Langley Research Center, Hampton, Virginia 23681 (alex.gloer-1@nasa.gov)

Abstract

The upper atmospheres of exoplanets are subject to two important energy sources derived from the host star. First, the stellar photon flux in the EUV and XUV ionizes and heats the upper atmosphere, driving atmospheric heating, affecting the conductance, and enhancing atmospheric escape. Second, the stellar wind's interaction with the planet's intrinsic magnetic field transfers energy to the atmosphere through field aligned currents and Poynting flux. That energy is dissipated in the high latitude cusp and auroral regions through Joule heating which can inflate the atmosphere and also enhance the escape rate. This presentation will discuss recent advances in modeling these energy inputs and their consequences for exoplanetary habitability.

1. Introduction

Recent Kepler observations revealed hundreds of terrestrial type exoplanets around G to M dwarfs. Many of the detected exoplanets are located close to their host stars and are exposed to large fluxes of ionizing radiation. How do exoplanetary atmospheres respond to such harsh stellar environments? This presentation discusses modeling the upper atmospheres of exoplanets with a focus on three key parts. Section 1.1 provides an overview of atmospheric escape processes and discusses how enhanced EUV and XUV inputs, typical for close-in exoplanets around active K-M dwarfs, may lead to significant atmospheric loss through the ionospheric outflow process. Section 1.2 presents recent results demonstrating how the extreme stellar wind conditions encountered by many exoplanets leads to enhanced Joule heating of those atmospheres and discusses the role of ionospheric conductivity in modulating the efficiencies of the energy

transfer from the wind to the planet. Finally, Section 1.3 discusses new model development to address these interesting problems including new calculations for ionospheric conductivity and upper atmospheric response.

1.1. Atmospheric Escape

Figure 1 presents a schematic summary of the different atmospheric escape processes. Many of these processes are independent of the planet's magnetic field. For example Jeans escape, which considers the portion of the distribution function above escape velocity, and hydrodynamic escape, a strong thermally driven bulk flow, have no terms related to the planet's field. On the other hand, the loss of atmosphere through collisional interaction with the stellar wind, known as sputtering, can be reduced when the planet has a strong field to shield the atmosphere from the influx of stellar wind particles. In contrast, ionospheric outflow can actually be enhanced by planetary magnetic fields as the field can collect and funnel energy from the wind into the planet.

In this presentation we will discuss atmospheric escape and its implication for atmospheric evolution. In particular, we will focus on recent results demonstrating how EUV and XUV inputs lead to atmospheric loss for close-in exoplanets such as Proxima Cen b [3, 1]. We show the scaling of ionized particle escape rates with XUV input and discuss the importance of thermospheric heating and magnetic field interactions.

1.2. Joule Heating

The habitable zone around faint M-dwarfs is very close to the star. While such conditions are favorable for detection, the extreme conditions encountered by this class of planets is extreme. In the case of TRAPPIST-1, planets e, f, and g are located at less than

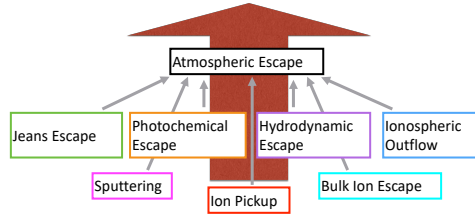


Figure 1: A schematic summary of the myriad of processes involved in atmospheric escape.

0.05 AU and are essentially inside the stellar corona. These stellar wind conditions may lead to heating and evaporation of the planetary atmosphere. Such conditions pose a challenge to whether such planets can truly be considered habitable. We present results from our recent paper examining the limits of the energy transmitted from the intense stellar wind to the upper atmosphere of the TRAPPIST-1 planets using an analytic formalism [2]. We explore the importance of the atmospheric conductivity in modulating the energy transmission and compare the energy transmission to other energy inputs from the star.

1.3. New Model Developments

In addition to the science results of the previous two section, we discuss new developments required for modeling energy input and effects in the upper atmospheres of exoplanets. In particular, we discuss improved approaches for calculating the conductivity and ohmic dissipation for exoplanet applications. We also present initial results of these new model developments.

Acknowledgments

This research study was supported by funding from the NASA NExSS The Living Breathing Planet project supported by NASA Astrobiology Institute and by the Sellers Exoplanetary Environments Collaboration at NASA GSGC & GISS.

References

- [1] Airapetian, V.S., Gloer, A., Khazanov, G.V., Loyd, R.O.P., France, K., Sojka, J., Danchi, W.C. and Liemohn, M.W., 2017. How hospitable are space weather affected habitable zones? The role of ion escape. *The Astrophysical Journal Letters*, 836(1), p.L3.
- [2] Cohen, O., Gloer, A., Garraffo, C., Drake, J.J. and Bell, J.M., 2018. Energy Dissipation in the Upper Atmospheres of TRAPPIST-1 Planets. *The Astrophysical Journal Letters*, 856(1), p.L11.
- [3] Garcia-Sage, K., Gloer, A., Drake, J.J., Gronoff, G. and Cohen, O., 2017. On the magnetic protection of the atmosphere of Proxima Centauri b. *The Astrophysical Journal Letters*, 844(1), p.L13.

Four years of upper atmospheric exploration at Mars with MAVEN and IUVS

Franck Montmessin (1), N. M. Schneider (2), J. I. Deighan (2), S. K. Jain (2), J. S. Evans (3), M. Crismani (2), M. H. Stevens, (4) D. Y. Lo (5), J. T. Clarke (6), M. S. Chaffin (2), M. Mayyasi (6), F. Lefèvre (1), A. Stiepen (2), E. Royer (2), Z. Milby (2), H. Groeller (5), R. Yelle (5), H. Nakagawa.

(1) LATMOS CNRS/UVSQ/UPMC/IPSL, Guyancourt/Paris, France, USA, (2) Laboratory for Atmospheric and Space Physics, University of Colorado at Boulder, (3) Computational Physics, Inc., (4) Space Science Division, Naval Research Laboratory, (5) Lunar and Planetary Lab, University of Arizona, (6) Center for Space Physics, Boston University, (7) Tohoku University, Japan (franck.montmessin@latmos.ipsl.fr).

Abstract

1. MAVEN's Imaging UltraViolet Spectrograph (IUVS)

The Mars Atmosphere and Volatile Evolution mission (MAVEN) is a Mars orbiter equipped with instruments to study the current state of the Mars atmosphere, atmospheric loss processes, and their fundamental drivers. Most instruments make *in situ* measurements of particles and fields in the Mars environment and upper atmosphere. IUVS is the only remote sensing instrument for the study of Mars' atmosphere and its interaction with the plasma environment [8]. The instrument has two main channels for the study of the upper atmosphere at far-UV and Mid-UV wavelengths, plus an echelle channel capable of spectrally resolving hydrogen and deuterium Lyman alpha lines to measure the D/H ratio [1]. The instrument uses a scan mirror to obtain limb scans or disk maps and is mounted on an Articulated Payload Platform (APP) which maintains Mars pointing while the spacecraft bus and solar arrays maintain sun-pointing. The spacecraft travels on an elliptical orbit allowing limb scans to be obtained at periapse and full-disk imaging at apoapse, and scans of Mars corona in between [3]. Thanks to the scan mirror, APP, and routine planning, the instrument observes with >50% duty cycles in a variety of repeating modes. On a bimonthly basis, the instrument performs two-day stellar occultation campaigns [5] to probe atmospheric structure.

2. Key science results

By virtue of broad instrument capabilities and extensive observations, IUVS has observed the vast majority of phenomena discovered by prior UV instruments, and revealed a significant number of

new phenomena as well. Observations of different phenomena can be individually optimized for spectral and two-dimensional resolution (through binning), as well as for sensitivity on daytime vs. night-time phenomena.

2.1 Dayglows and Nightglows

MAVEN/IUVS dayglow observations build on a rich history of prior UV studies by the Mariner missions and the SPICAM instrument on Mars Express. The dominant MUV emissions derive from solar excitation, ionization and dissociation of CO₂, and subsequent ionization and dissociation products. The brightest FUV emissions are atomic emissions from the constituent atoms of CO₂ and H₂O, plus additional molecular bands originating with CO₂ and its breakdown products. In addition to all spectral features observed by prior missions, IUVS has unambiguously observed and mapped the N₂ Vegard Kaplan bands [4, 11], and observed and mapped Mg⁺ from meteor ablation [2]. The instrument also recorded the aftermath of the most intense meteor shower observed with scientific instrumentation, after the close passage of Comet Siding Spring past Mars in October 2014 [9]. Limb scan dayglow observations have been powerful studies of spatial, seasonal and short-term variations in the thermosphere [6]. Longitudinal non-migrating tides have been observed in the peak emission altitudes [7].

The primary form of nightglow observed by IUVS is nitric oxide chemoluminescence. Nitrogen and oxygen atoms are liberated through molecular photodissociation on Mars' dayside. The atoms are then carried by thermospheric and mesospheric circulation patterns towards the winter pole, where they recombine and emit in the gamma and delta band of NO. IUVS limb scan observations [13] confirmed the basic geographic and seasonal

emissions distribution predicted by modelling and observed by MEX/SPICAM. These observations also showed that the observed latitudinal emission distribution was not as sharply peaked at the winter poles as in models, an indication the circulation models may be missing important processes. Wave-3 tides were observed in equatorial regions at some seasons. Further apoapse imaging work with broader local time coverage is likely to distinguish between migrating, nonmigrating and stationary waves, offering further insights on their origin.

2.2 H and D observations above the exobase

The MAVEN IUVS instrument contains an echelle spectrograph channel designed to measure D and H Ly α emissions from the upper atmosphere of Mars. This channel has successfully recorded both emissions, which are produced by resonant scattering of solar emission, over the course of most of a martian year. The fundamental purpose of these measurements is to understand the physical principles underlying the escape of H and D from the upper atmosphere into space, and thereby to relate present-day measurements of an enhanced HDO/H₂O ratio in the bulk atmosphere to the water escape history of Mars. Variations in these emissions independent of the solar flux reflect changes in the density and/or temperature of the species in the upper atmosphere. The MAVEN measurements show that the densities of both H and D vary by an order of magnitude over a martian year, and not always in synch with each other. This discovery has relevance to the processes by which H and D escape into space. One needs to understand the controlling factors to be able to extrapolate back in time to determine the water escape history from Mars at times when the atmosphere was thicker, when the solar flux and solar wind were stronger, etc. Further measurements will be able to identify the specific controlling factors for the large changes in H and D, which likely result in large changes in the escape fluxes of both species [16].

2.3 Stellar occultations

Stellar occultations are a well-established tool for retrieving vertical profiles of density, temperature and composition in Earth and planetary atmospheres. As stars rise or set behind a planet's atmosphere, gases (and aerosols, if present) absorb light with their individual spectroscopic signatures. CO₂ and O₃ are

the two gases readily identified in the IUVS wavelength range [5]. Thousands of occultation events have been observed by SPICAM on Mars Express [14] and vertical profiles have been used to understand and constrain models of the middle atmosphere [15]. To first order the vertical profile can reveal how the mesosphere has been raised, lowered or stretched out by heating or cooling processes. Statistically significant variations in the profiles are evidence of waves, tides or other perturbations.

IUVS has acquired data on Mars for more than one Martian year. During this time, beginning with March 2015 reported in [5], hundreds of stellar occultations have been since observed, during 12 dedicated occultation campaigns, executed on average every two to three months. The occultations cover the latitudes from 80°S to 75°N and the full range longitude, and local times with relatively sparse sampling. From these measurements we retrieve CO₂, O₂, and O₃ number densities as well as temperature profiles in the altitude range from 20 to 160 km, covering eight orders of magnitude in pressure from $\sim 2 \times 10^1$ to $\sim 4 \times 10^{-7}$ Pa. These data constrain the composition and thermal structure of the atmosphere. The O₂ mixing ratios retrieved during this study show a high variability from 1.5×10^{-3} to 6×10^{-3} ; however, the mean value seems to be constant with solar longitude. We detect ozone between 20 and 60 km. In many profiles there is a well-defined peak between 30 and 40 km with a maximum density of $1 - 2 \times 10^9$ cm⁻³. Examination of the vertical temperature profiles reveals substantial disagreement with models, with observed temperatures both warmer and colder than predicted. Examination of the altitude profiles of density perturbations and their variation with longitude shows structured atmospheric perturbations at altitudes above 100 km that are likely non-migrating tides. These perturbations are dominated by zonal wavenumber 2 and 3 with amplitudes greater than 45 %.

2.4 Ozone mapping

While ozone is mostly found closer to the surface of Mars, it also supplies information about the large-scale circulation phenomena that extends deep in the mesosphere. At every apoapsis, IUVS activates its built-in scan to assemble a global mosaic of Mars in the MUV range where ozone can be retrieved for each individual FOV. This permits an acute

characterization of ozone longitudinal and latitudinal behavior, providing unique insights into the short-term dynamical chemical processes at work in the ozone annual cycle.

3. Data Access

All data, including higher-level products are archived for public use at NASA's Planetary Data System (PDS). All team publications indicate the data types used and reference the time period(s) utilized in the analysis. An instrument description and data format document ("Software Interface Specification") is also provided at the PDS.

Acknowledgements

FM acknowledges the support of CNES, the French space agency, for his activities as MAVEN CoI.

References

- [1] Clarke, J.T. et al., "Variability of D and H in the Martian Upper Atmosphere Observed with the MAVEN IUVS Echelle Channel", *J. Geophys. Res. Space Physics*, 122, 2017.
- [2] Crismani, M. M. J. et al., "A persistent meteoric metal layer in the Martian atmosphere", *Nature Geoscience*, 10, 401–404, 2017.
- [3] Deighan, J., et al., MAVEN IUVS observation of the hot oxygen corona at Mars, *Geophys. Res. Lett.*, 42, 2015.
- [4] Evans, et al., Retrieval of CO₂ and N₂ in the Martian thermosphere using dayglow observations by IUVS on MAVEN, *Geophys. Res. Lett.*, 42, 2015.
- [5] Gröller, H., et al., "Probing the Martian atmosphere with MAVEN/IUVS stellar occultations", *Geophys. Res. Lett.*, 42, 2015.
- [6] Jain, S. K., et al., "The structure and variability of Mars upper atmosphere as seen in MAVEN/IUVS dayglow observations", *Geophys. Res. Lett.*, 42, 2015.
- [7] Lo, D.Y., et al., "Non-migrating tides in the Martian atmosphere as observed by MAVEN IUVS", *Geophys. Res. Lett.*, 42, 2015.
- [8] McClintock, W.E., et al., "The Imaging Ultraviolet Spectrograph (IUVS) for the MAVEN Mission", *Space Science Reviews*, 2015.
- [9] Schneider, N. M., et al., "MAVEN IUVS observations of the aftermath of the Comet Siding Spring meteor shower on Mars", *Geophys. Res. Lett.*, 42, 4755–4761, 2015.
- [10] Schneider, N.M., et al., "Discovery of diffuse aurora on Mars", *Science* 350, 2015.
- [11] Stevens, M.H. et al., "New observations of molecular nitrogen in the Martian upper atmosphere by IUVS on MAVEN", *Geophys. Res. Lett.*, 42, 2015.
- [12] Stevens, M.H. et al., "Martian Mesospheric Cloud Observations by IUVS on MAVEN", *Geophys. Res. Lett.*, 44, 2017
- [13] Stiepen, A., et al., "Nitric Oxide Nightglow and Martian Mesospheric Circulation from MAVEN/ IUVS Observations and LMD-MGCM Predictions", *J. Geophys. Res. Space Physics*, 122, 2017.
- [14] Montmessin, F., E. Quémerais, J.-L. Bertaux, O. Korablev, P. Rannou, and S. Lebonnois, Stellar occultations at UV wavelengths by the SPICAM instrument: Retrieval and analysis of Martian haze profiles, *J. Geophys. Res.*, 111, E09S09, doi:10.1029/2005JE002662, 2006.
- [15] Forget, F., F. Montmessin, et al., Density and temperatures of the upper Martian atmosphere measured by stellar occultations with Mars Express SPICAM, *J. Geophys. Res.*, 114, E01004, doi:10.1029/2008JE003086, 2009.
- [16] Mayyasi et al., (2017), The Variability of Atmospheric Deuterium Brightness at Mars: Evidence for Seasonal Dependence, *JGR*, 122, doi: 10.1002/2017JA024666

Mass-loss rate constraints on the observed distribution of exoplanets

Patricio Cubillos (1), Luca Fossati (1), Nikolai V. Erkaev (2), Ines Juvan (1), Colin P. Johnstone (3), Helmut Lammer (1), Monika Lendl (1), Petra Odert (1), and Kristina G. Kislyakova (3)

(1) Space Research Institute, Austrian Academy of Sciences, Graz, Austria, (2) Federal Research Center "Krasnoyarsk Science Center" SB RAS, "Institute of Computational Modelling", Krasnoyarsk, Russia, (3) Department of Astrophysics, University of Vienna, Vienna, Austria

Abstract

Atmospheric escape is a key factor shaping the known exoplanet population, determining their composition and size, among other properties. Here, we present a uniform analysis of the atmospheric escape rate of Neptune-like planets with known radius and mass. For each planet we characterize their mass-loss rate by computing the Jeans escape parameter (Λ), for a hydrogen atom evaluated at the planetary mass, radius, and equilibrium temperature. Values of $\Lambda \lesssim 20$ suggest extremely high mass-loss rates. For a sample of 170 Neptunes, we select the planets with high escape rates to further estimate their mass-loss rates (L_{hy}) with tailored atmospheric hydrodynamic models.

We find that nearly 15% of the planets exhibit extremely high mass-loss rates ($L_{\text{hy}} > 0.1 M_{\oplus} \text{Gyr}^{-1}$), which defy evolution and composition models of their atmospheres. On one hand, these mass-loss rates should deplete the planetary atmospheres from their hydrogen content within the first Gyr. On the other hand, the observed mass and radius lead to low densities, requiring a significant hydrogen envelope fraction.

To solve this contradiction, we hypothesize that these planets are not truly under such high mass-loss rates. Instead, either hydrodynamic models overestimate the mass-loss rates, transit-timing-variation measurements underestimate the planetary masses, optical transit observations overestimate the planetary radii (due to high-altitude clouds), or Neptunes have consistently higher albedos than Jupiter planets. We conclude that at least one of these established estimations/techniques is consistently producing biased values for Neptune planets. Such an important fraction of exoplanets with misinterpreted parameters can significantly bias our view of populations studies.

Energy balance in Saturn's upper atmosphere

Ingo C. F. Müller-Wodarg (1), Tommi T. Koskinen (2), Luke Moore (3) and Michael Mendillo (3)

(1) Imperial College London, UK, (2) University of Arizona, Tucson, USA, (3) Boston University, USA

(i.mueller-wodarg@imperial.ac.uk)

Abstract

Like for giant planets in our solar system, the energy balance in Saturn's upper atmosphere (its thermosphere) remains hitherto largely unknown, with temperatures exceeding the values expected from solar heating by 200–300 K [9]. Considerable energy is supplied to the polar regions via atmosphere-magnetosphere coupling processes, but General Circulation Models have highlighted the difficulty in distributing this energy on a fast spinning planet from pole to equator due to the strong Coriolis forces [7, 4]. Using the Saturn Thermosphere Ionosphere General Circulation Model (STIM) [3, 4, 2], we show that the addition of zonal momentum drag in the calculations can sufficiently reduce the Coriolis-barrier to allow for pole-to-equator transport of energy, thus producing a good match with the observed exospheric temperatures. Such momentum drag could result from the dissipation of atmospheric gravity waves recently identified from Cassini Ion and Neutral Mass Spectrometer (INMS) [8] observation in Saturn's thermosphere during the final proximal orbits [5]. The need for additional wave-induced momentum drag in upper atmosphere wind calculations has previously been highlighted for Earth [6] and Venus [1] and is in our study for the first time applied to a giant planet upper atmosphere model.

References

- [1] Bougher, S. W., R. G. Roble, R. E. Dickinson, and E. C. Ridley (1988). Venus mesosphere and thermosphere. III - Three-dimensional general circulation with coupled dynamics and composition, *Icarus*, 73, 545–573.
- [2] Moore, L., I. C. F. Müller-Wodarg, M. Galand, A. Kliore, and M. Mendillo (2010). Latitudinal variations in Saturn's ionosphere: Cassini measurements and model comparisons. *J. Geophys. Res.*, 115, A11317.
- [3] Müller-Wodarg, I. C. F., M. Mendillo, R. V. Yelle, and A. D. Aylward (2006). A global circulation model of Saturn's thermosphere *Icarus*, 180, 147–160.
- [4] Müller-Wodarg, I. C. F., L. Moore, M. Galand, S. Miller, and M. Mendillo (2012). Magnetosphere-atmosphere coupling at Saturn: 1. Response of thermosphere and ionosphere to steady state polar forcing, *Icarus*, 221, 481–494.
- [5] Müller-Wodarg, I. C. F., T. Koskinen, L. Moore, J. Serigano, R. V. Yelle, S. Hörst, J. H. Waite, and M. Mendillo (2018). Atmospheric Waves and their possible Effect on the Thermal Structure of Saturn's Thermosphere. *Under review, Geophys. Res. Lett.*
- [6] Schoeberl, M. R., and D. F. Strobel (1978) The Zonally Averaged Circulation of the Middle Atmosphere, *J. Atmos. Sci.* 35, 577–591.
- [7] Smith, C. G. A., A. D. Aylward, G. H. Millward, S. Miller, and L. E. Moore (2007) An unexpected cooling effect in Saturn's upper atmosphere, *Nature* 445, 399–401.
- [8] Waite, J. H., W. S. Lewis, W. T. Kasprzak, V. G. Anicich, B. P. Block, T. E. Cravens, G. G. Fletcher, W.-H. Ip, J. G. Luhmann, R. L. McNutt, H. B. Niemann, J. K. Parejko, J. E. Richards, R. L. Thorpe, E. M. Walter, and R. V. Yelle (2004). The Cassini Ion and Neutral Mass Spectrometer (INMS) Investigation. *Sp. Sci. Rev* 114, 113–231.
- [9] Yelle, R. V. and S. Miller (2004). Jupiter's thermosphere and ionosphere, in "Jupiter: Planet, Satellites & Magnetosphere", F. Bagenal, W. McKinnon, and T. Dowling eds. *Cambridge University Press* 185–218.

Results and thoughts on H_3^+ observations of solar system giant planets

James O'Donoghue (1), Henrik Melin (2), Luke Moore (3), Tom Stallard (2)

(1) NASA Goddard Space Flight Center, Greenbelt, United States (j.odonoghue@nasa.gov), (2) University of Leicester, Leicester, UK, (3) Boston University, Boston MA, USA

Abstract

The upper atmospheres of Jupiter, Saturn and Uranus consist of a quasi-neutral ionosphere co-located with a neutral (mostly hydrogen) thermosphere. One of the major ions of the ionosphere is H_3^+ (read: *Aitch three plus*) is a remarkably useful probe of these environments, with it's near IR emissions revealing the ion's line-of-sight column-averaged temperature, column density and total radiative cooling rate to space. H_3^+ is considered to be approximately in local thermodynamic equilibrium to it's surroundings, and therefore H_3^+ temperatures are representative of the upper-atmospheric temperature as a whole. In addition to this major scientific benefit, H_3^+ also emits at a range of convenient Earth and Gas Giant atmospheric windows, such that it can be readily observed using ground- and space-based platforms.

In this presentation we will detail how we observe H_3^+ and highlight the major results of the past 30 years at Jupiter, Saturn and Uranus. In addition, we will highlight recent results which show that the Great Red Spot heats the upper atmosphere above it, and that it's raining on Saturn and the rings are responsible. We will also discuss what H_3^+ can tell us about exoplanets, should it be detected at them and attempt to answer the general question:

“Could we see Jupiter's upper-atmospheric H_3^+ from Alpha Centauri?”

Ground-based observations of hot exoplanet upper atmospheres

Aurélien Wyttenbach (1,2)

(1) Leiden University, Leiden Observatory, Netherlands, (2) Geneva University, Geneva Observatory, Switzerland
(aurelien.wyttenbach@unige.ch)

Abstract

Transiting exoplanets are among the best suitable targets for atmospheric studies, particularly with transmission spectroscopy. This technique studies the light filtered through the atmosphere of an exoplanet, as it passes in front of its star. These observations have experienced a rapid development in the last few years, allowing us to precisely probe the low part of atmospheres. Despite these progresses, we are still unable to understand the link between the low and the upper part of atmospheres, with the latter undergoing evaporation.

Transit observations from the ground with stabilised high-resolution spectrograph, such as HARPS, have key roles to play in this context. Indeed, while taking care of multiple challenges linked to the stellar lines variability (Rossiter-McLaughlin effect, center-to-limb variation, activity), studies of sodium lines (via the Fraunhofer D doublet) deliver innovative measurements of atmospheres. The measured sodium absorptions in the atmospheres of several hot Jupiters have revealed new informations about their thermospheres. The thermosphere is a very specific region of intermediate altitudes (very low pressure), where most of the stellar irradiation is absorbed by atoms and molecules, resulting in an upper atmospheric heating. This mechanism potentially lead to a hydrodynamical expansion of the atmosphere that may trigger the exoplanet evaporation. The classical sodium probe is now joined with a few other probes (such as Helium) increasing the possibilities to measure this part of the upper atmosphere. Henceforth, observations at high-resolution, particularly in the optical and infrared domain (e.g. with ESPRESSO, CARMENES, etc.), are a valuable and important resource in order to understand exoplanets atmospheres.